ACTA MECHANICA SINICA, Vol.20, No.1, February 2004
The Chinese Society of Theoretical and Applied Mechanics
Chinese Journal of Mechanics Press, Beijing, China
Allerton Press, INC., New York, U.S.A.

ISSN 0567-7718

LIQUEFACTION AND DISPLACEMENT OF SATURATED SAND UNDER VERTICAL VIBRATION LOADING*

LU Xiaobing (鲁晓兵)[1,†] TAN Qingming (谈庆明)[1] CHENG C. M. (郑哲敏)[1]
YU Shanbing (俞善炳)[1] CUI Peng (崔 鹏)[2]

[1](*Institute of Mechanics, Chinese Academy of Sciences, Beijing* 100080, *China*)
[2](*Institute of Mountain Hazard and Environment, Chinese Academy of Sciences, Chengdu* 610041, *China*)

ABSTRACT: In order to investigate the influence of the vertical vibration loading on the liquefaction of saturated sand, one dimensional model for the saturated sand with a vertical vibration is presented based on the two phase continuous media theory. The development of the liquefaction and the liquefaction region are analyzed. It is shown that the vertical vibration loading could induce liquefaction. The rate of the liquefaction increases with the increase of the initial limit strain or initial porosity or amplitude and frequency of loading, and increases with the decrease of the permeability or initial modulus. It is shown also that there is a phase lag in the sand column. When the sand permeability distribution is non-uniform, the pore pressure and the strain will rise sharply where the permeability is the smallest, and fracture might be induced. With the development of liquefaction, the strength of the soil foundation becomes smaller and smaller. In the limiting case, landslides or debris flows could occur.

KEY WORDS: liquefaction, vibration loading, fracture, saturated sand

1 INTRODUCTION

It is practical to study the development of liquefaction either to prevent the liquefaction hazard or to consolidate sand foundations. For example, when a vibration loading such as a wave loading is applied on a saturated soil foundation, liquefaction may occur under some conditions. The liquefied foundation has a small strength and so can slide or flow even with a very small slope. Since it is considered that the liquefaction is caused by earthquake through the shear action, much attention and efforts have been paid on shear responses of the saturated sand and a series of results have been obtained[1,2]. Considering the coupling of the shear loading and the vertical loading, much work has been done about the wave propagation and the development of the pore pressure in the saturated sand[3,4]. Those studies are helpful to understanding liquefaction, but the sustaining pore pressure is thought to be caused by shear only. Recently, some results on liquefaction of seabed under the vertical vibrating loading and laterally confined conditions have been obtained[5~7]. Nevertheless, the skeleton of sands is taken often as elastic and the discussion is rather about the development of the pore pressure or effective stress than the expansion of the liquefaction region. Therefore, in order to study the liquefaction characteristics under a vertical vibration, the following problem is to be considered in building an one dimensional strain model: The sand layer extends infinitely horizontally and finitely vertically (Fig.1). The sand characteristics only change vertically. The vibration loading is applied on the top of the sand layer through water while the bottom is fixed. The saturated sand is at the static state before the vibration is applied on. By this model the development of the liquefaction and some other dynamic responses under the vertical vibration will be studied.

Received 3 June 2002, revised 20 May 2003
* The project supported by the National Natural Science Foundation of China (40025103, 10202024)
† E-mail: xblu@imech.ac.cn

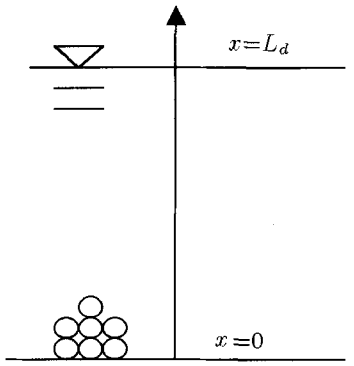

Fig.1 The sketch of the problem ($x = 0 : v_s = v_w = 0$; $x = L_d : p = A_1 \sin(2\pi ft)$, $\sigma_e = 0$)

2 THE BASIC EQUATIONS

The basic equations of the saturated sand consist of the constitutive relation, conservation equations and initial and boundary conditions.

2.1 The Constitutive Relation

The pressure confined constitutive relation is adopted[8], which is based on the consolidation experiments. This constitutive relation consists of a loading part and an unloading part and is expressed as follows:

the loading part

$$\sigma_e - \sigma_{ers} = \frac{E_{rs}(\varepsilon - \varepsilon_{rs})}{1 + \dfrac{\varepsilon - \varepsilon_{rs}}{\varepsilon_{rls}}} \tag{1}$$

the unloading part

$$\sigma_e - \sigma_{efs} = \frac{E_{fs}(\varepsilon - \varepsilon_{fs})}{1 + \dfrac{\varepsilon - \varepsilon_{fs}}{\varepsilon_{fls}}} \tag{2}$$

in which $\sigma_{ers}, \sigma_{efs}, \varepsilon_{rs}, \varepsilon_{fs}$ are the stress and the strain at the starting point of the loading part and the unloading part, respectively, and $E_{rs}, E_{fs}, \varepsilon_{rls}, \varepsilon_{fls}$ are the tangent modulus and the limit strain of the loading part and the unloading part, respectively.

The tangent modulus and the limit strain of the loading part can be expressed as

$$E_{rs} = E_{r0}\left(1 + \frac{\varepsilon_{rs}}{a_1 + a_2\varepsilon_{rs}}\right)\left(1 + \frac{\sigma_{ers}}{\sigma_{ec}}\right)^{0.5} \tag{3}$$

$$\varepsilon_{sr} = \varepsilon_{rl0}\left(1 - \frac{\varepsilon_r}{a_3 + a_4\varepsilon_r}\right)\left(1 + \frac{\sigma_{er}}{\sigma_{ec}}\right)^{0.5} \tag{4}$$

in which $E_{r0}, \varepsilon_{rl0}$ are the initial tangent modulus and limit strain of the loading curve, respectively, $a_1 \sim a_4$ are empirical constants, $\varepsilon_{rs}, \sigma_{ers}$ are, respectively, the stress and the strain of the starting point of the loading curve of No. s, σ_{ec} is the pre-consolidation stress and is equal to 1.0 kPa.

Similarly, the tangent modulus and the limit strain of the unloading part can be expressed as

$$E_{fs} = E_{r0}\left(1 + \frac{\varepsilon_{fs}}{b_1 + b_2\varepsilon_{fs}}\right)\left(1 + \frac{\sigma_{efs}}{\sigma_{ec}}\right)^{0.5} \tag{5}$$

$$\varepsilon_{fls} = \varepsilon_{rl0}\left(1 - \frac{\varepsilon_{fs}}{b_3 + b_4\varepsilon_{fs}}\right)\left(1 + \frac{\sigma_{efs}}{\sigma_{ec}}\right)^{0.5} \tag{6}$$

in which $b_1 \sim b_4$ are experimental constants. The examples of experiments are shown in Fig.2.

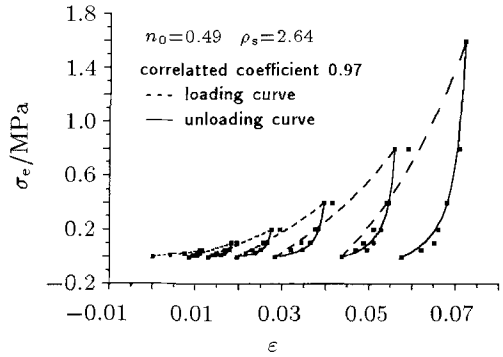

(a) Comparison of experimental data and fitted curves of sample No.1

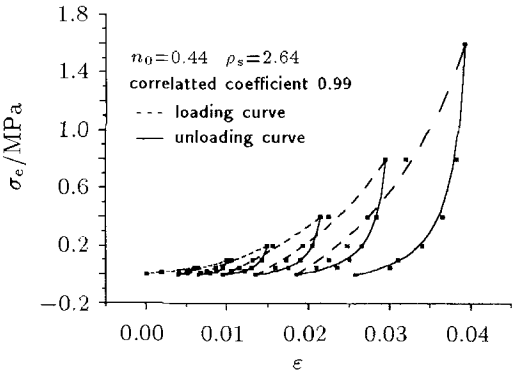

(b) Comparison of experimental data and fitted data of sample No.2

Fig.2 The fitted curves and experimental data

All empirical constants in Eqs.(1)~(6) are obtained from fitting of the experimental data.

2.2 The Conservation Equations and the Initial and Boundary Conditions

The governing equations of the saturated sand were first established for dynamic phenomena by Biot[9] and some analytical results were obtained[10].

Afterwards, the governing equations based on the mixture theory were proposed[11,12], but they did not reprsent any substantial or rational change in comparison with Biot's equations. Owing to the increasing interest in nonlinear applications, some controlling equations of incremental form were derived by Zienkiewicz[13] and Prevost[14,15] et al. However, the equations taking the displacements as the basic variables are not convenient for the analysis in this paper and the assumption that water and grains are both compressible is not necessary. So assuming water is compressible because of air in it, a one dimensional system of equations of the saturated sand under vertical vibration is used as follows[16]

$$\begin{aligned}
&n\beta\frac{\partial p}{\partial t}+\rho_{\mathrm{w}}\frac{\partial n}{\partial t}+n\rho_{\mathrm{w}}\frac{\partial v_{\mathrm{w}}}{\partial x}+\rho_{\mathrm{w}}v_{\mathrm{w}}\frac{\partial n}{\partial x}+\\
&\quad nv_{\mathrm{w}}\beta\frac{\partial p}{\partial x}=0\\
&\frac{\partial n}{\partial t}-(1-n)\cdot\frac{\partial v_{\mathrm{s}}}{\partial x}+v_{\mathrm{s}}\cdot\frac{\partial n}{\partial x}=0\\
&n\rho_{\mathrm{w}}\cdot\frac{\partial v_{\mathrm{w}}}{\partial t}+n\frac{\partial p}{\partial x}=-H+n\rho_{\mathrm{w}}g\\
&(1-n)\cdot\rho_{\mathrm{s}}\cdot\frac{\partial v_{\mathrm{s}}}{\partial t}+(1-n)\cdot\frac{\partial p}{\partial x}+\frac{\partial\sigma_{\mathrm{e}}}{\partial x}=\\
&\quad H+(1-n)\rho_{\mathrm{s}}g
\end{aligned}\tag{7}$$

in which n is the porosity, $v_{\mathrm{w}}, v_{\mathrm{s}}$ are, respectively, the velocities of water and grains, ρ_{w} is the density of water, ρ_{s} is the density of grains, p is the pore pressure, σ_{e} is the effective stress, β is the compressibilily coefficient of water, g is the gravity acceleration, H represents the interaction between water and grains and is assumed as

$$H=n^2(v_{\mathrm{w}}-v_{\mathrm{s}})/K \tag{8}$$

in which $K=k/\mu$, μ and k are the viscosity of water and the permeability, respectively.

The geometric relations connecting the velocity of grains v_{s} and the strain ratio $\dot{\varepsilon}$, and the relation between the interaction coefficient K and the porosity n are assumed as follows

$$\dot{\varepsilon}=\frac{\partial v_{\mathrm{s}}}{\partial x} \tag{9}$$

$$K=\left(\frac{n}{n_0}\right)^5\left(\frac{1-n_0}{1-n}\right)^2K_0 \tag{10}$$

in which K_0 is the initial interaction coefficient when the initial porosity of sand is n_0[17].

The initial conditions are

$$\begin{aligned}
&t=0 && n=f_1(x)\\
&p=\rho_{\mathrm{w}}g\cdot x && \sigma_{\mathrm{e}}=(1-n_0)(\rho_{\mathrm{s}}-\rho_{\mathrm{w}})g\cdot x\\
&v_{\mathrm{w}}=v_{\mathrm{s}}=0
\end{aligned}\tag{11}$$

in which $f_1(x)$ is the distribution function of the initial porosity.

The boundary conditions are

$$\begin{aligned}
&x=L_d && p=A_1\sin(2\pi ft) && \sigma_{\mathrm{e}}=0\\
&x=0 && v_{\mathrm{s}}=v_{\mathrm{w}}=0
\end{aligned}\tag{12}$$

in which A_1, f are the amplitude and the frequency of the loading on the boundary, L is the region of the sand layer.

Now, a set of first order difference scheme for mass and momentum conservation is established as follows

$$\begin{aligned}
&n_i^j\beta(p_i^j-p_i^{j-1})+\rho_{\mathrm{w}i}^j(n_i^j-n_i^{j-1})+\\
&\quad\rho_{\mathrm{w}i}^jn_i^j(v_{\mathrm{w}i}^j-v_{\mathrm{w}i-1}^j)\frac{\Delta t}{\Delta x}+\rho_{\mathrm{w}i}^jv_{\mathrm{w}i}^j(n_i^j-n_{i-1}^j)\frac{\Delta t}{\Delta x}+\\
&\quad n_i^jv_{\mathrm{w}i}^j\beta(p_i^j-p_{i-1}^j)\frac{\Delta t}{\Delta x}=0\\
&n_i^j-(1-n_i^j)(v_{\mathrm{s}i}^j-v_{\mathrm{s}i-1}^j)\frac{\Delta t}{\Delta x}+\\
&\quad v_{\mathrm{s}i}^j(n_i^j-n_{i-1}^j)\frac{\Delta t}{\Delta x}=n_i^{j-1}\\
&(\rho_{\mathrm{w}}+K_i^j\Delta tn_i^j)v_{\mathrm{w}i}^j-K\Delta tn_i^jv_{\mathrm{s}i}^j+\frac{\Delta t}{\Delta x}p_i^j-\\
&\quad\frac{\Delta t}{\Delta x}p_{i-1}^j=\rho_{\mathrm{w}}v_{\mathrm{w}i}^{j-1}+\rho_{\mathrm{w}}g\\
&\left[1-n_i^j+K(n_i^j)^2\right]v_{\mathrm{s}i}^j-K\Delta t(n_i^j)^2v_{\mathrm{w}i}^j+\\
&\quad\frac{\Delta t(1-n_i^j)}{\Delta x}p_i^j-\frac{\Delta t(1-n_i^j)}{\Delta x}p_{i-1}^j=D
\end{aligned}\tag{13}$$

in which i, j are, respectively, the space step and the time step, and

$$\begin{aligned}
&D=K(1-n_i^j)v_{\mathrm{s}i}^j+\frac{\sigma_{\mathrm{e}i-1}^j-\sigma_{\mathrm{e}i}^j}{\Delta x}+(1-n_i^j)g\\
&\rho_{\mathrm{w}i}^j=\beta(p_i^j-p_i^0)+\rho_{\mathrm{w}0}
\end{aligned}\tag{14}$$

The difference schemes of the geometry relationship between velocity v_{s} and strain ratio $\dot{\varepsilon}$ are

$$\dot{\varepsilon}_i^{j-1}=\left(v_{\mathrm{s}i}^{j-1}-v_{\mathrm{s}i-1}^{j-1}\right)/\Delta x \tag{15}$$

$$\varepsilon_i^j=\varepsilon_i^{j-1}+\dot{\varepsilon}\Delta t \tag{16}$$

The difference scheme of the initial conditions are

$$j=0 \qquad n_i^j = f_{1i}^j(x)$$
$$p_i^j = \rho_w g \cdot x_i \qquad \sigma_{ei} = (1-n_0)(\rho_s - \rho_w) g \cdot x_i \quad (17)$$
$$v_{wi}^j = v_{si}^j = 0$$

The difference scheme of the boundary conditions are

$$x = L \quad p_i^j = A_2 \sin(2\pi f \cdot j \cdot \Delta t) \quad \sigma_{ei}^j = 0 \quad (18)$$
$$x = 0 \quad v_{si}^j = 0 \quad v_{wi}^j = 0 \quad (19)$$

3 THE COMPARISON OF OUR COMPUTED RESULTS WITH THOSE OF NOGO

Nogo[6] has designed a one dimensional laterally confined experiment to study liquefaction of seabed under water oscillation. The bottom is fixed. The inner diameter of the column is 8.9 cm while the height is 2.1 m. The other parameters are as follows: the density of grains is ρ_s, the porosity n, the permeability k, the thickness of sand D, the mean water pressure over head h_0 (hydrostatic pressure head), the amplitude of the pressure variation in the head a_0, the frequency of the pressure variation f. The values of parameters in Nogo's experiments are

$$n_0 = 0.4 \qquad \rho_s = 2.65 \times 10^3 \,\mathrm{kg/m^3}$$
$$f = 1.37\,\mathrm{Hz} \qquad a_0 = 40\,\mathrm{cm}$$
$$h_0 = 100\,\mathrm{cm} \qquad k = 1.5 \times 10^{-11}\,\mathrm{m^2}$$
$$D = 100\,\mathrm{cm}$$

Here we adopt the same data in our computation.

The computed results are compared with the data of Nogo[6] in Fig.3. A generally good agreement between them can be seen when the skeleton is taken as elastic.

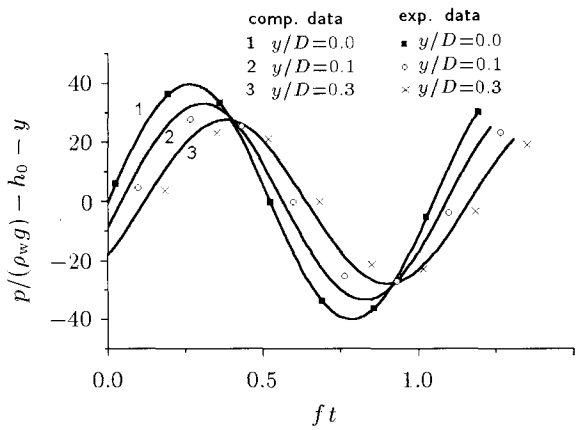

Fig.3 Comparison of our computed results with the data of Nogo

4 THE CHANGES OF THE EFFECTIVE STRESS

The changes of the effective stress are summarized in this section. The parameters adopted are as follows:

The initial tangent modulus $E_{r0} = (0.51 \sim 5.1)\,\mathrm{MPa}$, the initial limit strain $\varepsilon_{rl0} = 0.1 \sim 0.7$,the initial permeability $(5 \times 10^{-11} \sim 5 \times 10^{-12})\,\mathrm{m^2}$,the initial porosity $n_0 = 0.35 \sim 0.55$, the amplitude of the loading $A_1 = (0.26 \sim 1.02)\,\mathrm{MPa}$, the frequency of the loading $f = (1 \sim 40)\,\mathrm{Hz}$.

It is shown that the change rate of the effective stress increases with the increase of the initial limit strain or the porosity or with the decrease of the modulus or the permeability, and increases with the increase of the amplitude or the frequency of the loading (Figs.4~9). As we know, if the modulus is small or the initial limit strain or the porosity is large or the amplitude of the loading is large and the frequency is high, the compressible tendency of the skeleton is large, and the permeability is small, it will be difficult for the pore water to drain and the pore pressure will rise and the effective stress will drop.

Figures 10 and 11 describe the pore pressure changes influenced by the permeability and the loading amplitude. It is shown that the pore pressures increase slowly at the beginning and then increase fast up to the maximum which is equal to the sum of the initial pore pressure and the initial effective stress(after liquefaction, the fluctuating pore pressure caused by the loading is not considered.). The increase rates of the pore pressure become faster and faster with the decrease of the permeability and with the increase of the loading amplitude.

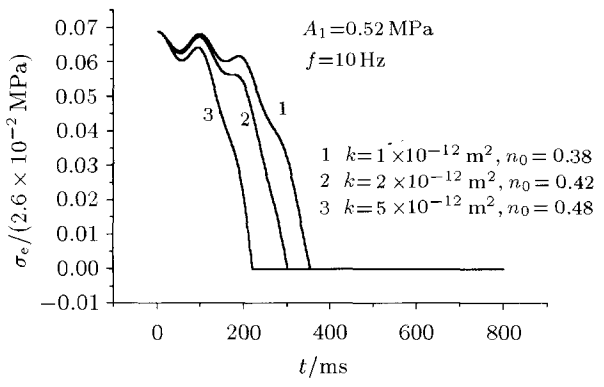

Fig.4 The influence of the permeability on the change of the effective stress

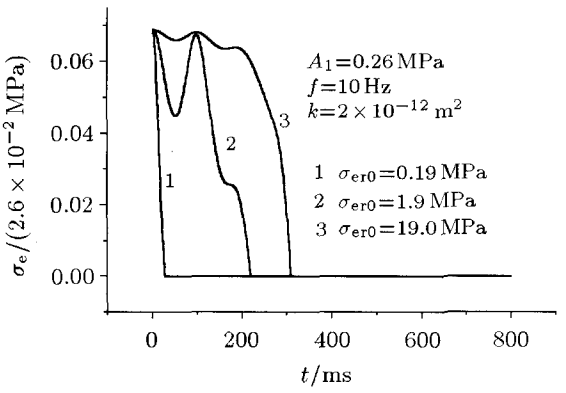

Fig.5 The influence of the initial tangent modulus on the change of the effective stress

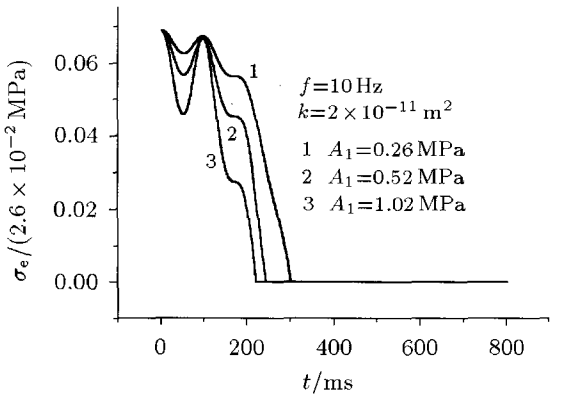

Fig.8 The influence of the amplitude of the loading on the change of the effective stress

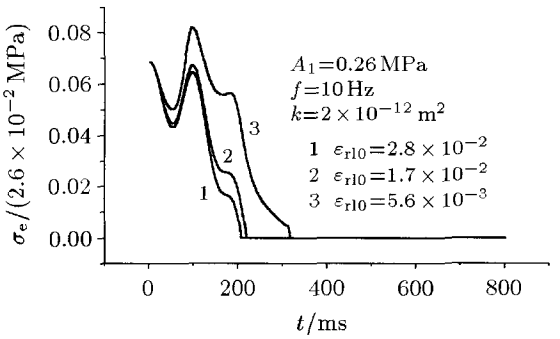

Fig.6 The influence of the initial limit strain on the change of the effective stress

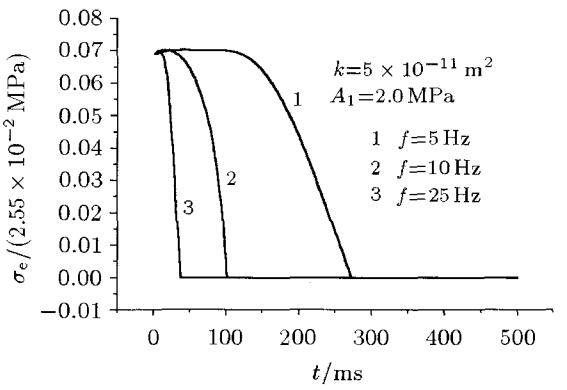

Fig.9 The influence of the frequency of the loading on the change of the effective stress

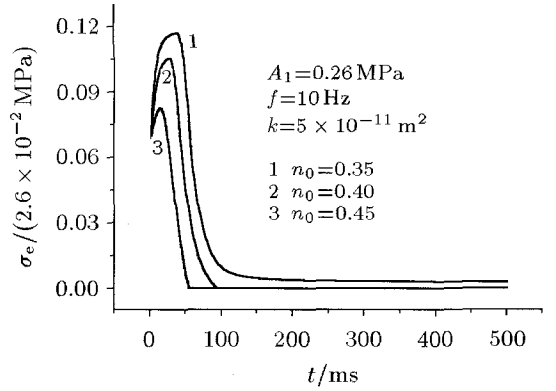

Fig.7 The influence of the initial porosity on the change of the effective stress

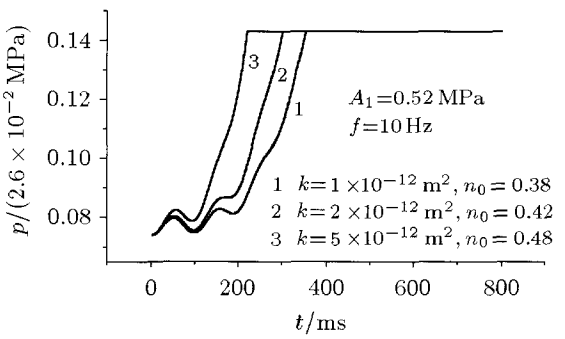

Fig.10 The influence of the permeability on the pore pressure

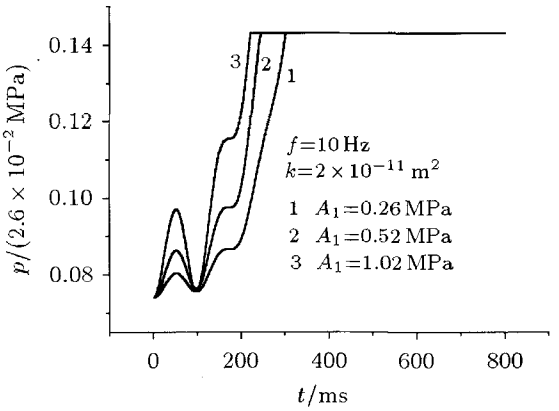

Fig.11 The influence of the amplitude on the pore pressure

5 THE RESPONSES OF STRESSES WITH DEPTH

When the permeability at $z = 1.0$ m is 10% or even 5% smaller than that at other points, the supper pore pressure and the strain will rise sharply and concentrate near the point with the smallest permeability (Figs.12 and 13). Since the supper pore pressure and the strain rise the fastest, this point will reach the failure state the earliest and the fracture of the sand column may ensue. It agrees with the main characteristics of the experiments[18~21] and the theoretical analysis[22].

Figure 14 gives the difference between the total stress increment at any point in the sand layer and that at the end of the loading(the total stress at time t minus that at time $t = 0$: $\sigma_e|_z + p|_z - \sigma_e|_0 - p|_0$) with time. It is shown that the amplitude increment of the total stress changes significantly, at the same time, the phase lag is obvious. Figure 15 gives the relation between the increment of the total stress with time and the amplitude of the loading. It is shown that the larger the amplitude of the loading, the larger the amplitude changes of the total stress in the saturated sand. Therefore, only when the loading is so small that the inertial of the sand may be neglected, the changes of the total stress with depth may be neglected.

Figures 16 and 17 give the changes of the velocities of water and soil v_w, v_s with the depth. It is shown that the two velocities change greatly near the boundary where the load is applied on. The waves of the two velocities degrade gradually with the depth. It may be seen that the two velocities are not always in the same directions at the same time, the reverse movements of two phases may play a role on the damage of the soil structure.

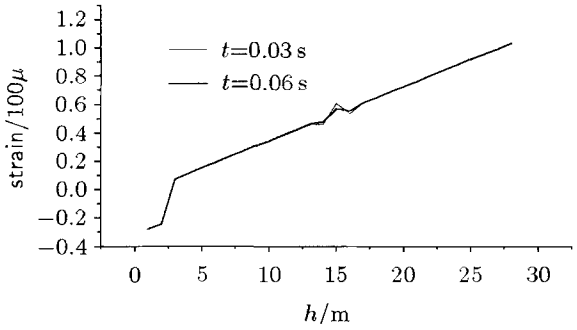

Fig.12 The changes of the strain along the depth

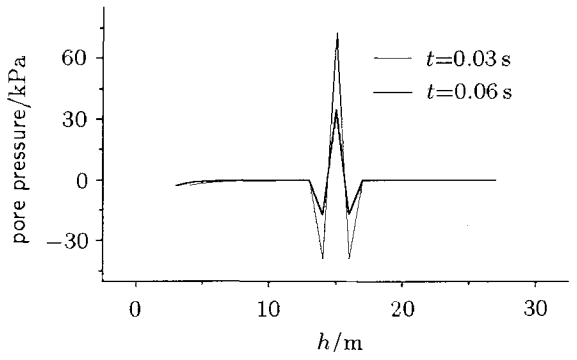

Fig.13 The changes of the supper pore pressure along the depth

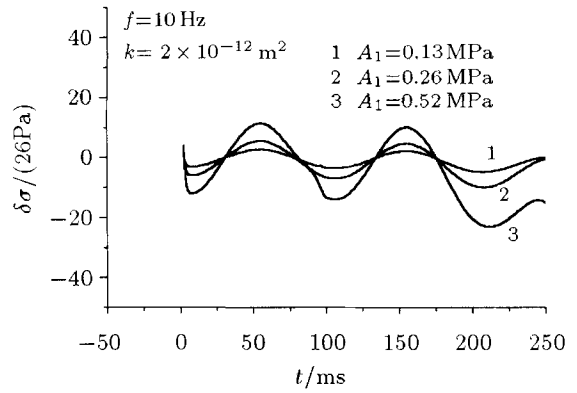

Fig.14 The difference between the total stress increment at any point and that at the boundary under different loads

Figure 18 gives the results of the pore pressure distribution along the depth at different times. It is shown that the biggest increment of the pore pressure is near the end of the loading and reduces gradually along the depth. Figure 19 gives the results of the effective stress distribution along the depth. It is shown that the effective stress decreases with time and deve-

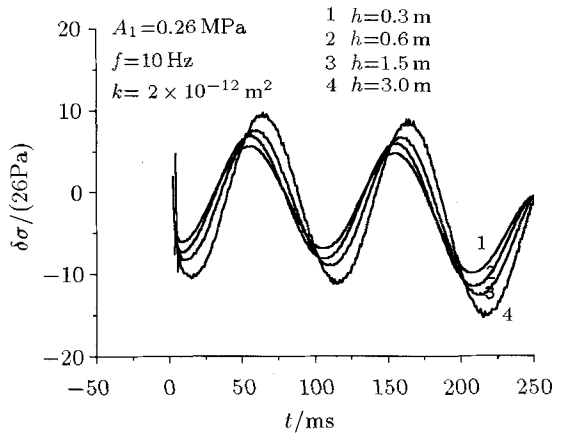

Fig.15 The difference between the total stress increment at any point in the sand and that at the boundary

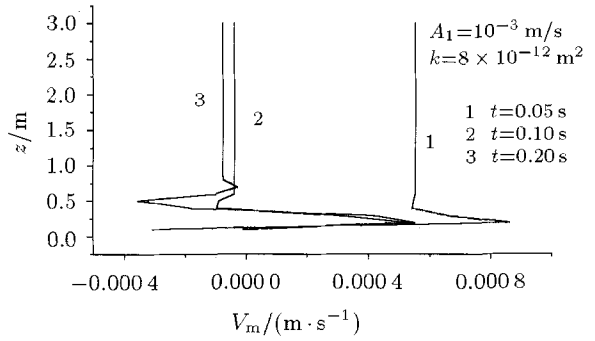

Fig.16 The velocity of water versus the depth

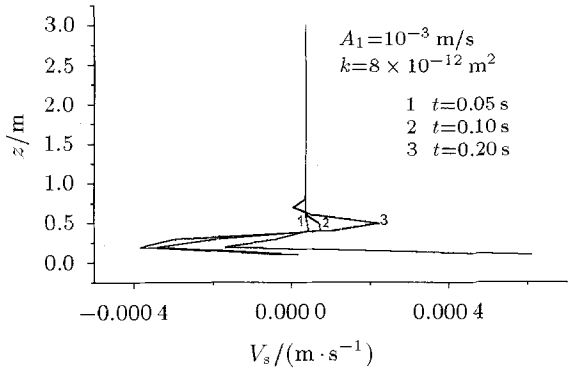

Fig.17 The velocity of grains versus the depth

lops along the depth gradually. The liquefaction zone forms first near the end of the loading and gradually develops along the depth. The data in those two figures are the mean values. Figure 20 gives the result

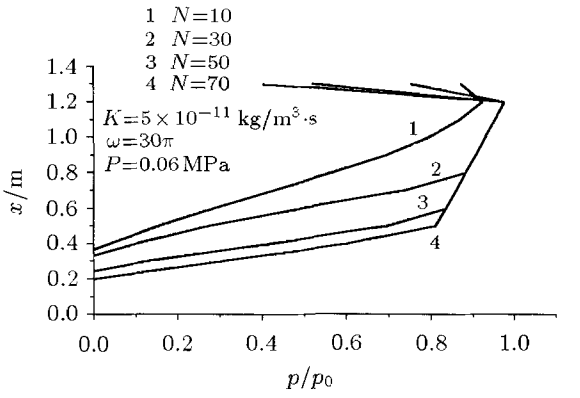

Fig.18 The pore pressure versus the depth

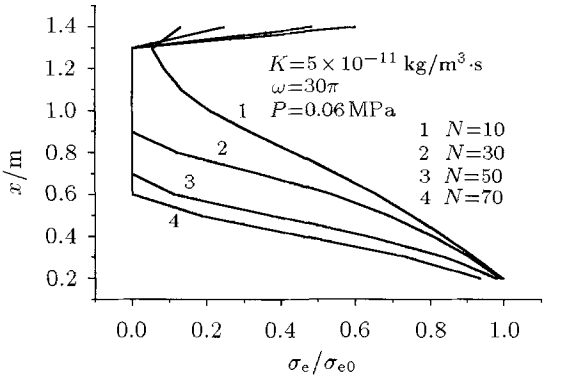

Fig.19 The effective stress versus the depth

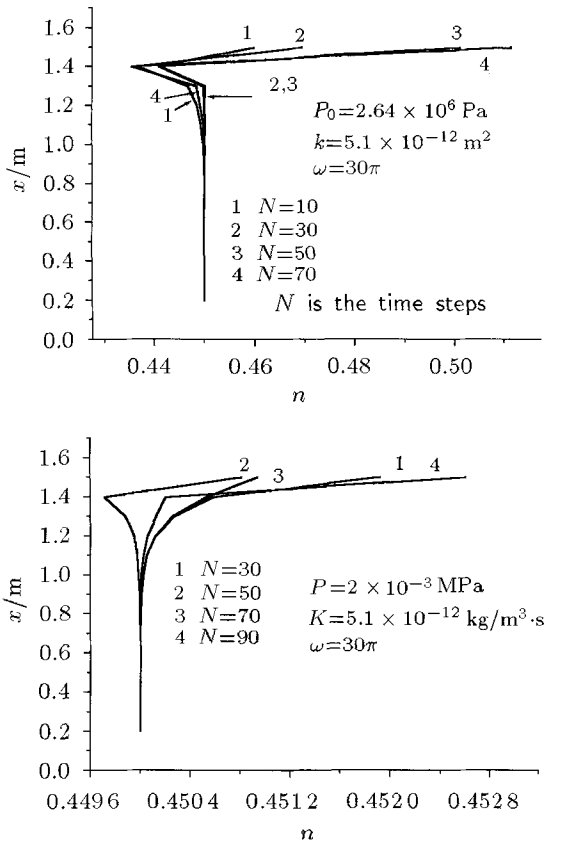

Fig.20 The porosity versus the depth

of the porosity distribution at different times. It is shown that the porosity changes significantly near the end of the loading. The porosities increase first and then decrease. It is because there is not enough time for the water to drain first and then it may drain with the time elapse.

6 THE INFLUENCES OF FACTORS ON EXPANSION OF LIQUEFACTION REGION

The influences of the controlling parameters on the development of the liquefaction region are discussed. These parameters include the permeability, initial tangent modulus, initial limit strain, initial porosity, amplitude and frequency of the loading. The variation of the liquefaction region L with the time t for different parameters are shown in Figs.21 through 26. The expansion of the liquefaction region increases with the decrease of the permeability or initial tangent modulus, and with the increase of the initial limit strain or the amplitude or frequency of loading.

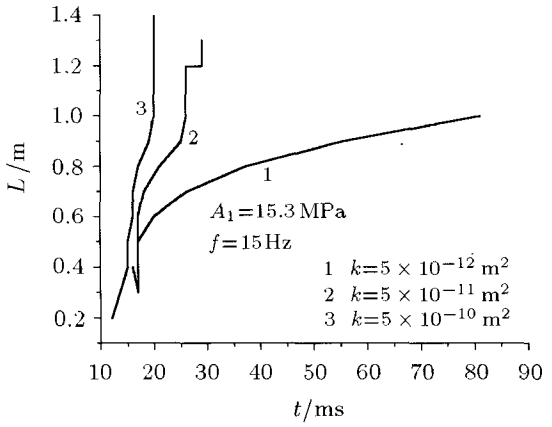

Fig.21 The influence of the permeability

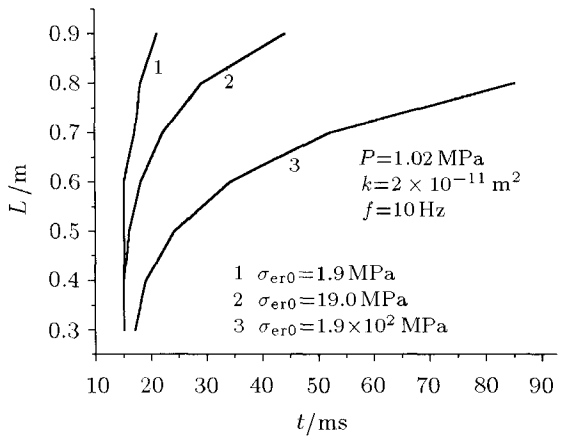

Fig.22 The influence of the initial tangent modulus

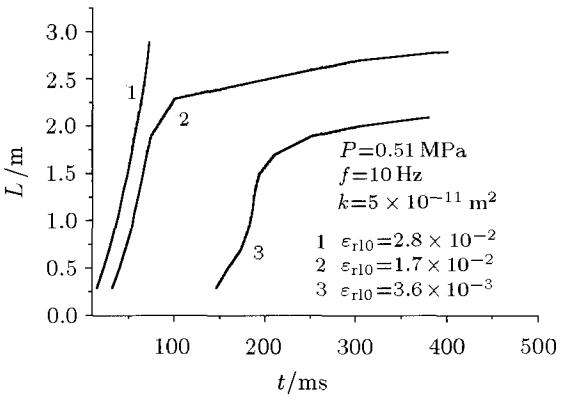

Fig.23 The influence of the initial limit strain

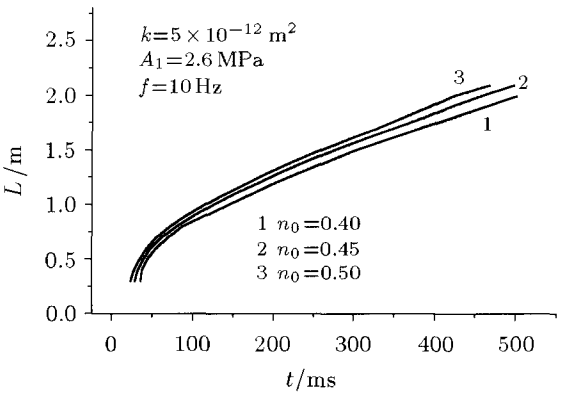

Fig.24 The influence of the initial porosity

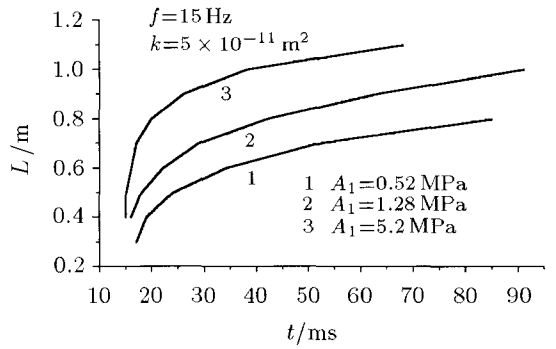

Fig.25 The influence of the amplitude of the loading

It is shown from the L-t curves in these figures that the liquefaction appears first near the end of the loading and forms the first liquefaction region, then it develops along the depth of the sand. Nevertheless, the damping in the saturated sand makes the influence weaker and weaker along the depth of the sand so that the developing rate of the liquefaction region decreases gradually to zero. At this time, the height of the liquefaction region reaches the maximum.

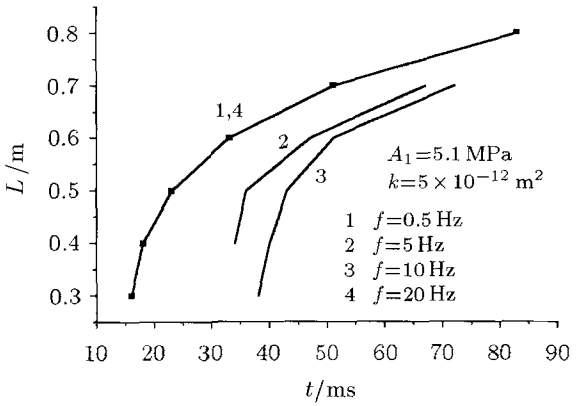

Fig.26 The influence of the frequency of the loading

As we know, the interaction between water and grains is strong and it is difficult for the pore water to drain if the permeability is small, so the development of the liquefaction region is fast. If the initial tangent modulus is small or the initial limit strain and the initial porosity are big, the structure is loose and the strength of the skeleton is small, the liquefaction will be easy to occur. If the amplitude of the loading is big and the frequency is high, the force that the saturated sand has to bear is big, the development of the liquefaction region will be fast.

The liquefactions caused by a pure shear loading and under laterally confined conditions are both the results of the strength loss and structure damage of the skeleton. But the liquefaction under laterally confined conditions cannot occur if the water and grains are both incompressible and the other end is fixed. The deformation of the sand skeleton is controlled by the laterally confined constitutive relation. On the other hand, it is controlled by the shear stress-strain relation under pure shear.

7 CONCLUSIONS

The main conclusions are as follows:

(1) Based on the two phase continuum media theory, the basic equations are obtained for the saturated sand under the one dimensional vertical vibration loading.

(2) The numerical analysis shows that the saturated sand may liquefy under the vibration loading. The dropping rate of the effective stress increases with the decrease of the permeability or the initial tangent modulus or with the increase of the amplitude or frequency of the loading or the initial porosity. The expansion of the liquefaction region will stop gradually.

(3) The total stress and the pore pressure will decrease and have a phase lag along the depth of the sand layer because of the damping of the saturated sand.

(4) If the permeability is non-uniform, the pore pressure and the strain will rise sharply and concentrate near the place where the permeability is the smallest. This might be the reason why the fracture occurs in the sand column.

REFERENCES

1 Finn WDL, Lee KW, Martin GR. An effective stress model for liquefaction. *J Geotech & Geoenviron ASCE*, 1977, 103(6): 517~533

2 Liou CP, Streeter VL. The numerical model of liquefaction. *Journal of the Geotechnical Engineering Division, ASCE*, 1977, 103(4): 589~606

3 Zienkiewicz OC, Shiomi T. Dynamic behaviour of saturated porous media; the generalized Biot formulation and its numerical solution. *International Journal for Numerical and Analytical Methods in Geomechanics*, 1984, 8: 71~96

4 Prevost JH. Nonlinear transient phenomenon in saturated porous media. *Computing Methods in Applied Mechanical Engineering*, 1982, (20): 3~8

5 Zen K, Yamazaki H. Oscillatory pore pressure and liquefaction in seabed induced by ocean waves. *Sands and Foundations*, 1990, 30(4): 147~161

6 Nogo H, Maeno S. Pore pressure and effective stresses in a highly saturated sand bed under water pressure variation on its surface. *Natural Disaster Science*, 1987, 9(1): 23~35

7 Hideo Sekiguchi, Katsutoshi Kita, Osamu Okamoto. Response of poro-elastoplastic beds to standing waves. *Sands and Foundations*, 1995, 35(3): 31~42

8 Lu XB. The analysis on liquefaction of saturated sand under vertical vibration loading. [PhD Thesis], Institute of Mechanics, Chinese Academy of Sciences, Beijing, 1999

9 Biot MA. Theory of propagation of elastic waves in a fluid-saturated porous solid. *J Acoust Soc Am*, 1956, 28: 168~191

10 Biot MA. Mechanics of deformation and acoustic propagation in porous media. *J Appl Phys*, 1962, 33: 1482~1498

11 Green AE, Naghdi PM. A dynamical theory of interacting continua. *Int J Eng Sci*, 1965, 3: 231~241

12 Green AE. On flow of fluid through an elastic solid. *Acta Mech*, 1970, 9: 329~340

13 Zienkiewicz OC, Chang CT, Bettess P. Drained, undrained, consolidating and dynamic behaviour assumptions in sands: limits of validity. *Geotechnique*, 1980, 30: 385~395

14 Provest JH. Mechanics of continuous porous media. *Int J Eng Sci*, 1980, 18: 787~800

15 Provest JH. Nonlinear transient phenomena in saturated porous media. *Comp Meth in Appl Mech Eng*, 1982, 20: 3~8

16 Yu SB. Steady development of coal-gas outbursts. *Acta Mechanica Sinica*, 1988, 20(2): 97~106

17 Huang WX. The Engineering Properties of Soils. Beijing: Hydraulic & Electrolic Press, 1983, 86~87 (in Chinese)

18 Peng FJ, Tan QM, Cheng CM. Laboratory study on cracks in saturated sands. *Acta Mechnica Sinica*, 2000, 16(1): 48~53

19 Zhang JF, Meng XY, Tan QM, et al. Experimental study on permeability and settlement of saturated sand under impact load. *Acta Mechanica Sinica*, 1999, 31(2): 230~237 (in Chinese)

20 Fiegel GL, Kutter BL. Liquefaction mechanism for layered soils. *J Geotech Engrg, ASCE*, 1994, 120(4): 737~755

21 Kobusho T. Water film in liquefied sand and its effect on lateral spread. *J Geotech and Geoenviron Engrg, ASCE*, 1999, 125(10): 817~826

22 Cheng CM, Tan QM, Zhang JF, et al. Study on the formation of horizontal cracks in saturated sand. Invited paper, In: Proc Explomet 2000, Albuquerque, New Mexico, USA, 2000